

The following resources related to this article are available online at <http://stke.sciencemag.org>.  
This information is current as of 13 December 2011.

- Article Tools** Visit the online version of this article to access the personalization and article tools:  
<http://stke.sciencemag.org/cgi/content/full/sigtrans;4/203/ra87>
- Supplemental Materials** "Supplementary Materials"  
<http://stke.sciencemag.org/cgi/content/full/sigtrans;4/203/ra87/DC1>
- References** This article cites 47 articles, 22 of which can be accessed for free:  
<http://stke.sciencemag.org/cgi/content/full/sigtrans;4/203/ra87#otherarticles>
- Glossary** Look up definitions for abbreviations and terms found in this article:  
<http://stke.sciencemag.org/glossary/>
- Permissions** Obtain information about reproducing this article:  
<http://www.sciencemag.org/about/permissions.dtl>

# Triggering Actin Comets Versus Membrane Ruffles: Distinctive Effects of Phosphoinositides on Actin Reorganization

Tasuku Ueno,<sup>1\*</sup> Björn H. Falkenburger,<sup>2†</sup> Christopher Pohlmeier,<sup>1</sup> Takanari Inoue<sup>1‡</sup>

A limited set of phosphoinositide membrane lipids regulate diverse cellular functions including proliferation, differentiation, and migration. We developed two techniques based on rapamycin-induced protein dimerization to rapidly change the concentration of plasma membrane phosphatidylinositol 4,5-bisphosphate [PI(4,5)P<sub>2</sub>]. First, using a membrane-recruitable form of PI(4)P 5-kinase, we increased PI(4,5)P<sub>2</sub> synthesis from phosphatidylinositol 4-phosphate [PI(4)P] and found that COS-7, HeLa, and human embryonic kidney 293 cells formed bundles of motile actin filaments known as actin comets. In contrast, a second technique that increased the concentration of PI(4,5)P<sub>2</sub> without consuming PI(4)P induced membrane ruffles. These distinct phenotypes were mediated by dynamin-mediated vesicular trafficking and mutually inhibitory crosstalk between the small guanosine triphosphatases Rac and RhoA. Our results indicate that the effect of PI(4,5)P<sub>2</sub> on actin reorganization depends on the abundance of other phosphoinositides, such as PI(4)P. Thus, combinatorial regulation of phosphoinositide concentrations may contribute to the diversity of phosphoinositide functions.

## INTRODUCTION

Complexity in signaling networks is often derived from a limited set of molecules that are co-opted for multiple tasks. Understanding how cells achieve such sophisticated processing using a finite set of molecules within a confined space is critical to understanding their biology. A paradigmatic example of such multitasking molecules is phosphatidylinositol 4,5-bisphosphate [PI(4,5)P<sub>2</sub>], a member of the phosphoinositide family of membrane lipids that is produced by means of the phosphorylation of phosphatidylinositol 4-phosphate [PI(4)P] by PI(4)P 5-kinase [PI(4)P5K]. Long known as a component of the cellular plasma membrane (PM), where it constitutes 1 to 2% of total lipids, PI(4,5)P<sub>2</sub> has recently been identified as a second messenger that can trigger such diverse cellular functions as membrane trafficking, ion channel activation, cytokinesis, phagocytosis, and cell migration (1–8). Consistent with this pleiotropic role, a series of lipid kinases and phosphatases dynamically control the concentration of PI(4,5)P<sub>2</sub> with high spatiotemporal precision in response to various stimuli (9). Mutations in genes encoding these enzymes result in various human diseases, including renal, neuromuscular, and developmental disorders; many types of cancers; and diabetes (10, 11). However, the question of how this single lipid can drive multiple cellular functions remains unresolved.

The technical difficulty of rapidly and specifically manipulating PI(4,5)P<sub>2</sub> in living cells has contributed to this lack of understanding. Rapid and inducible manipulation of membrane lipids can help identify the direct consequences of the perturbation by avoiding the possible compensations often observed among these membrane lipids (12, 13).

To begin to understand the multiple roles of PI(4,5)P<sub>2</sub> at the molecular level, we developed a technique to rapidly manipulate PI(4,5)P<sub>2</sub> concentration based on the rapamycin-triggered dimerization of FKBP506-binding protein (FKBP) and FKBP–rapamycin-binding (FRB) protein and used it to study dynamic actin phenotypes such as ruffles and comets. Ruffles provide the driving force for the motility of various cell types, including leukocytes, lymphocytes, fibroblasts, epithelial cells, and neurons (14). They are often observed at the leading edge of migrating cells where they develop into pseudopodia. In contrast, endocytic vesicles can be rapidly propelled through the cell by actin comet tails (15), suggesting that they facilitate vesicular trafficking. Using the FKBP-FRB dimerization technique, we can rapidly target a protein of interest to a predetermined intracellular location, thereby inducing changes in the activity of various signaling molecules on a time scale of seconds (16). Here, we describe using this approach to manipulate phosphoinositides and to distinguish between the effects of increasing the concentration of PI(4,5)P<sub>2</sub> and decreasing that of PI(4)P, which is a signaling molecule in its own right (17).

## RESULTS

### PI(4,5)P<sub>2</sub> concentration can be increased in cells independently of its synthesis from PI(4)P

We used two approaches to increase the concentration of PI(4,5)P<sub>2</sub>. In the first approach, we anchored FRB at the PM by means of an N-terminal signal sequence from a Lyn kinase (Lyn<sub>11</sub>-FRB) and used rapamycin to rapidly recruit a YFP (yellow fluorescent protein)–FKBP–PI(4)P5K construct to the PM to phosphorylate PI(4)P (Fig. 1). When the Lyn<sub>11</sub>-FRB labeled with cyan fluorescent protein (CFP) (Lyn<sub>11</sub>-CFP-FRB) and YFP-FKBP-PI(4)P5K were transfected in COS-7 cells, YFP-FKBP-PI(4)P5K translocated from the cytosol to the PM on a time scale of seconds upon addition of rapamycin (Fig. 2A and movie S1).

In the second approach, we developed a technique that we call PI(4,5)P<sub>2</sub> “liberation,” which increases PI(4,5)P<sub>2</sub> without decreasing PI(4)P (Fig. 1). Much of PI(4,5)P<sub>2</sub> at the PM is bound to proteins (18). We fused the

<sup>1</sup>Department of Cell Biology, Center for Cell Dynamics, School of Medicine, Johns Hopkins University, Baltimore, MD 21205, USA. <sup>2</sup>Department of Physiology and Biophysics, School of Medicine, University of Washington, Seattle, WA 98195, USA.

\*Present address: Graduate School of Pharmaceutical Sciences, University of Tokyo, Tokyo 113-0033, Japan.

†Present address: Department of Neurology, RWTH Aachen University, 52074 Aachen, Germany.

‡To whom correspondence should be addressed. E-mail: jctinoue@jhmi.edu

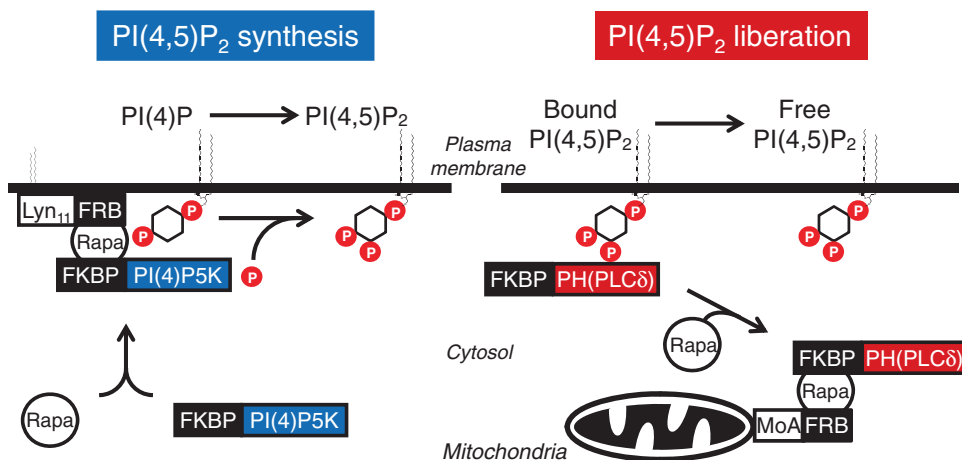


**Fig. 1.** Schematic illustration of two techniques to rapidly manipulate PI(4,5)P<sub>2</sub> by chemically inducible dimerization. PI(4,5)P<sub>2</sub> synthesis from PI(4)P: Rapamycin recruits cytosolic FKBP-PI(4)P5K to the plasma membrane (PM) where FRB is anchored through a myristoylation and palmitoylation modification sequence, by formation of the tripartite FRB-rapamycin-FKBP complex. This places PI(4)P5K near its substrate PI(4)P, enabling PI(4)P phosphorylation at the D5 position to produce PI(4,5)P<sub>2</sub>. PI(4,5)P<sub>2</sub> liberation: Before addition of rapamycin, FKBP-PH(PLCδ) preferentially localizes at the PM through its interaction with PI(4,5)P<sub>2</sub>. Rapamycin recruits FKBP-PH(PLCδ) from the PM to mitochondria, where FRB is anchored via the transmembrane motif of MoA.

pleckstrin homology (PH) domain of phospholipase C-δ (PLCδ) to FKBP tagged with fluorescent protein (FP) to create a PI(4,5)P<sub>2</sub>-binding protein [FKBP-PH(PLCδ)] and used rapamycin to rapidly remove FKBP-PH(PLCδ) from the PM, thus increasing the amount of free PI(4,5)P<sub>2</sub>. We recruited FKBP-PH(PLCδ) to FRB anchored at the cytosolic surface of mitochondria through the transmembrane motif of monoamine oxidase A (MoA). We chose mitochondria because they are the second largest intracellular organelle and thereby provide sufficient capacity to sequester FKBP-PH(PLCδ) and because they have little role in phosphoinositide signaling (19).

To determine whether the FKBP modification affected the PI(4,5)P<sub>2</sub>-binding property of PH(PLCδ), we coexpressed YFP-FKBP-PH(PLCδ) with a non-FKBP-modified form of PH(PLCδ), CFP-PH(PLCδ). Like CFP-PH(PLCδ), YFP-FKBP-PH(PLCδ) localized to the PM (fig. S1A), supporting the previous report that PI(4,5)P<sub>2</sub> preferentially exists at the PM (20). When we stimulated cells with platelet-derived growth factor (PDGF) to activate endogenous PLC, which cleaves PI(4,5)P<sub>2</sub>, FKBP-PH(PLCδ) transiently dissociated from the PM, with kinetics and extent similar to those of CFP-PH(PLCδ) (fig. S1B). Thus, the FKBP modification did not appear to alter the efficacy of PI(4,5)P<sub>2</sub> binding by PH(PLCδ).

When FKBP-PH(PLCδ) was transfected together with mitochondria-targeted FRB (FRB-MoA) for PIP<sub>2</sub> liberation, rapamycin induced the rapid translocation of FKBP-PH(PLCδ) from the PM to mitochondria (Fig. 1B and movie S2).

To evaluate PI(4,5)P<sub>2</sub> concentration at the PM in response to PI(4,5)P<sub>2</sub> synthesis or PI(4,5)P<sub>2</sub> liberation, we measured current through KCNQ2 and 3 (KCNQ2/3) potassium channels, which is known to scale with PI(4,5)P<sub>2</sub> concentration but is insensitive to PI(4)P (12, 21–25). We first confirmed that KCNQ2/3 current increases with PI(4,5)P<sub>2</sub> synthesis, as previously shown (12), and also with PI(4,5)P<sub>2</sub> liberation (fig. S2, A to D, and E, left bar). In contrast, sequestration of a phosphatidylserine-binding protein such as the C2 domain of lactadherin [FKBP-C2(Lact)] from the PM to mitochondria did not lead to a marked increase in KCNQ2/3 current [right bar in fig. S2E;

$P < 0.05$  for sequestration of FKBP-C2(Lact) compared to that of FKBP-PH(PLCδ)]. Subsequently, we used KCNQ4 channels, which have lower affinity for PI(4,5)P<sub>2</sub> (26) and are thus less likely to be saturated with increasing PI(4,5)P<sub>2</sub>. KCNQ4 current increased with PI(4,5)P<sub>2</sub> synthesis and PI(4,5)P<sub>2</sub> liberation by  $74 \pm 13\%$  and  $46 \pm 7\%$ , respectively (Fig. 1, C and D), confirming that PI(4,5)P<sub>2</sub> increases with both manipulations. The time course of FKBP-PH(PLCδ) translocation to the mitochondria, as determined by Förster resonance energy transfer (FRET) between YFP on FKBP-PH(PLCδ) and CFP on FRB-MoA, coincided with that of the increase in KCNQ current (Fig. 1D and fig. S2). The similar time course and extent of the increase in PI(4,5)P<sub>2</sub> with the two manipulations were reproduced by a computational simulation (fig. S2, F and G, and tables S1 and S2) using previously established parameters of phosphoinositide metabolism (22).

We used total internal reflection fluorescence (TIRF) microscopy, using the PH domain of oxysterol-binding protein (OSBP) labeled with FP as a PI(4)P biosensor [FP-PH(OSBP)] (27), to evaluate the effects of

both manipulations on PI(4)P. TIRF microscopy measures fluorescence signals originating from the PM and its immediate vicinity but not from deeper in the cytoplasm. We found that GFP (green fluorescent protein)-PH(OSBP) rapidly dissociated from the PM upon membrane recruitment of PI(4)P5K, but not of a catalytically inactive D253A mutant form [PI(4)P5K-KD] (Fig. 1E), consistent with depletion of its substrate PI(4)P. In contrast, the GFP-PH(OSBP) signal was unaffected by PI(4,5)P<sub>2</sub> liberation (Fig. 1F). On the basis of our computational simulation of PI(4,5)P<sub>2</sub> liberation (fig. S2G), which is informed by experimental measurements of PH(PLCδ) translocation and PI(4,5)P<sub>2</sub> metabolism (22), we expected that a fraction of the liberated PI(4,5)P<sub>2</sub> might be dephosphorylated into PI(4)P by ambient 5-phosphatases. However, if this small PI(4)P increase occurred, it did not result in a visible translocation of FP-PH(OSBP) to the PM.

### PI(4,5)P<sub>2</sub> synthesis and PI(4,5)P<sub>2</sub> liberation induce distinct actin phenotypes

To evaluate the effects of the rapid PI(4,5)P<sub>2</sub> manipulations on the actin cytoskeleton, we used a regulator of actin assembly, Ena/VASP (vasodilator-stimulated phosphoprotein), labeled with FP (FP-Ena/VASP-like, or FP-Evl) that can visualize various types of actin structures (28). Using confocal fluorescence microscopy imaging of FP-Evl in living cells, we confirmed that recruitment of PI(4)P5K to the PM robustly induced actin comets (Fig. 3A and movie S3). We failed to observe actin comet formation when PI(4)P5K-KD was recruited to the membrane (fig. S3), indicating that a catalytic reaction [that is, PI(4,5)P<sub>2</sub> synthesis] is responsible for comet formation. In contrast, PI(4,5)P<sub>2</sub> liberation through sequestration of FKBP-PH(PLCδ) from the PM to the mitochondria did not elicit the formation of actin comets, but instead induced membrane ruffling (Fig. 3B and movie S4). When PI(4,5)P<sub>2</sub> liberation was achieved through sequestration of a different (4,5)P<sub>2</sub>-binding protein, Tubby (2, 29), cells exhibited the same ruffling phenotype (fig. S4, A and B). However, sequestration of a phosphatidylserine-binding protein [FKBP-C2(Lact)] from the PM to mitochondria did not elicit membrane ruffling (fig. S4, C and D).

Actin comets are preferentially generated from lipid rafts (30). To determine whether the distinct actin phenotypes we observed with PI(4,5)P<sub>2</sub> synthesis and its liberation were due to the PI(4,5)P<sub>2</sub> production at different membrane domains, we created a construct in which FRB was fused to a K-Ras CAAX tail [as a PM-targeting sequence that is not associated with any particular domain (31)] instead of Lyn<sub>11</sub>, which is thought to be associated with lipid rafts (31). We observed that PI(4,5)P<sub>2</sub> synthesis achieved with the FRB-CAAX construct resulted in the same actin comet

phenotype as that associated with Lyn<sub>11</sub>-FRB (fig. S3). The actin comets and ruffles induced by these PI(4,5)P<sub>2</sub> manipulations were also apparent with phalloidin staining of fixed cells in which FP-Evl was not overexpressed (fig. S5) and were consistently observed in different cell types, including HEK293T and HeLa cells (fig. S6).

Overexpression of PH(PLCδ) sequesters substantial amounts of PI(4,5)P<sub>2</sub> and alters some aspects of PI(4,5)P<sub>2</sub> signaling and metabolism (32). Therefore, the cells used to investigate the effects of PI(4,5)P<sub>2</sub>

liberation might show aberrant PI(4,5)P<sub>2</sub> signaling before addition of rapamycin [and independent of PI(4,5)P<sub>2</sub> liberation]. Similarly, overexpression of FKBP-PI(4)P5K may increase PI(4,5)P<sub>2</sub> signaling despite the deliberate mislocalization of the FKBP-PI(4)P5K construct to the cytoplasm (12). To exclude these possibilities, we conducted PI(4,5)P<sub>2</sub> synthesis or PI(4,5)P<sub>2</sub> liberation in the presence of overexpressed PH(PLCδ) or PI(4)P5K, respectively. In both cases, we observed the predicted actin phenotypes (that is, actin comets with synthesis or membrane ruffles with liberation, respectively) (Fig. 3, C and D). Occurrence of the actin phenotypes induced by the two different PI(4,5)P<sub>2</sub> manipulations appeared to be mutually exclusive (Fig. 3E).

### Crosstalk between Rho family guanosine triphosphatases regulates PI(4,5)P<sub>2</sub>-induced actin remodeling

Next, we addressed the molecular mechanisms that give rise to these distinct actin phenotypes. The Rho family of guanosine triphosphatases (GTPases), which include Rac, Cdc42, and RhoA, act as molecular switches capable of orchestrating actin dynamics (14, 33). The activity of the Rho GTPases is regulated by phosphoinositides (33), suggesting that they could provide a link between our manipulations of phosphoinositide concentration and the actin phenotypes we observed. Therefore, we used constitutively active or dominant-negative mutants of Rho GTPases to dissect the mechanisms underlying the PI(4,5)P<sub>2</sub>-induced actin phenotypes. Constitutively active Rac or Cdc42 significantly attenuated PI(4,5)P<sub>2</sub> synthesis-induced formation of actin comets (Fig. 4A,  $P < 0.01$ ; see table S3), whereas dominant-negative mutants of Rac or Cdc42 did not affect actin comet formation. This combination suggests that Rac and Cdc42 are not required for comet formation but that the activity of Rac and Cdc42 must be suppressed for comet formation. Neither constitutively active nor dominant-negative forms of RhoA affected actin comet formation (Fig. 4A), suggesting that either RhoA does not play a role in comet

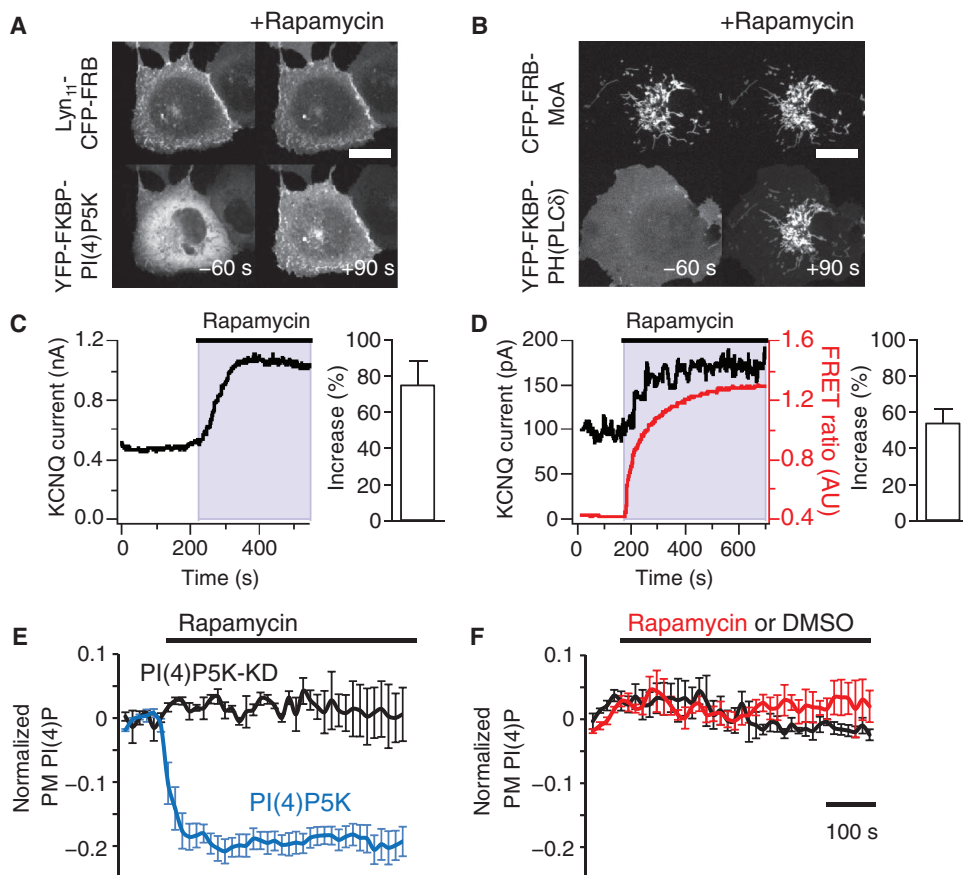


**Fig. 2.** PI(4,5)P<sub>2</sub> concentration is increased in cells independently of its synthesis from PI(4)P by PI(4,5)P<sub>2</sub> liberation. (A and B) Time series confocal fluorescence microscopy images of COS-7 cells coexpressing either Lyn<sub>11</sub>-CFP-FRB and YFP-FKBP-PI(4)P5K to achieve PI(4,5)P<sub>2</sub> synthesis (A) or CFP-FRB-MoA and YFP-FKBP-PH(PLCδ) to achieve PI(4,5)P<sub>2</sub> liberation (B). Cell images were collected every 15 s and are shown before (−60 s) and after (90 s) addition of rapamycin (100 nM). Scale bars, 20 μm. (C and D) Currents through KCNQ4 potassium channels transfected in tSA201 cells were elicited by depolarization from −60 to −20 mV for 300 ms and quantified as tail current amplitude. Note that the density of expressed channels varies considerably between cells (21). (C) Expression of KCNQ4 with the components for PI(4,5)P<sub>2</sub> synthesis. (D) Expression of KCNQ4 with the components for PI(4,5)P<sub>2</sub> liberation. Translocation of YFP-PH(PLCδ) to CFP-FRB-MoA is simultaneously reported by FRET (YFP emission with CFP excitation/CFP emission with CFP excitation) from the same cells. Bar graphs in (C) and (D) represent summary data (means ± SEM) of the percent increase in KCNQ4 tail current in response to rapamycin treatment for  $n = 7$  cells for PI(4,5)P<sub>2</sub> synthesis and  $n = 9$  cells for PI(4,5)P<sub>2</sub> liberation. (E and F) TIRF measurements of PM PI(4)P with PI(4,5)P<sub>2</sub> manipulation. Normalized fluorescence intensity of GFP-PH(OSBP) was collected every 15 s from COS-7 cells expressing Lyn<sub>11</sub>-FRB with mCherry-FKBP-PI(4)P5K (blue) or mCherry-FKBP-PI(4)P5K-KD (gray) (E), where rapamycin was added on the 60th second. Normalized fluorescence intensity of GFP-PH(OSBP) for COS-7 cells expressing FRB-MoA and mCherry-FKBP-PH(PLCδ) with addition of rapamycin (red) or dimethyl sulfoxide (DMSO) (0.1%, gray) (F).  $\Delta F/F_0$  indicates fluorescence change divided by initial fluorescence ( $n = 3$ ). Error bars indicate SEM.



formation or RhoA is activated through suppression of Rho GTPase-activating proteins (GAPs). To test the latter possibility, we inhibited the RhoA downstream effector Rho-associated kinase (ROCK). In the presence of the ROCK inhibitor Y-27632, we observed phenotype conversion; cells exhibited membrane ruffling and diminished actin comet formation with PI(4,5)P<sub>2</sub> synthesis (Fig. 4, B and C). This suggests that ROCK activity (and, therefore, RhoA signaling) is required for formation of actin comets and may need to be suppressed for membrane ruffling. Y-27632 administration over long periods of time can decrease PI(4,5)P<sub>2</sub> synthesis, suggesting that PI(4)P5K could be a downstream target of Rho-ROCK signaling (34).

However, we observed no effect of Y-27632 on the recovery of KCNQ2/3 currents after rapid PI(4,5)P<sub>2</sub> dephosphorylation at the D5 position, one measure of PI(4)P5K activity (22) (fig. S7), supporting the hypothesis that ROCK acts downstream of PI(4,5)P<sub>2</sub>.

In contrast to their lack of effect on comet formation with PI(4,5)P<sub>2</sub> synthesis, dominant-negative Rac or Cdc42 suppressed membrane ruffling in response to PI(4,5)P<sub>2</sub> liberation (Fig. 4D), suggesting that Rac and Cdc42 are necessary for this process. Both constitutively active and dominant-negative forms of RhoA suppressed membrane ruffling in response to PI(4,5)P<sub>2</sub> liberation, suggesting that either a cycle of guanosine diphosphate (GDP)–guanosine triphosphate (GTP) exchange is required for ruffle formation or there is a narrow concentration window at which active RhoA promotes ruffle formation (35). In the presence of dominant-negative Rac, cells developed actin comets in response to PI(4,5)P<sub>2</sub> liberation (Fig. 4, E and F). Together with the ruffles observed in response to PI(4,5)P<sub>2</sub> synthesis in the presence of the ROCK inhibitor (Fig. 4, B and C), these phenotypic conversions underline the mutually exclusive actin phenotypes shown in Fig. 3E.

To further characterize the pathways, we visualized the dynamics of actin-binding proteins such as N-WASP and cofilin, major participants in PI(4,5)P<sub>2</sub>-dependent actin reorganization (8). N-WASP accumulated at the tip of comets in response to PI(4,5)P<sub>2</sub> synthesis, whereas cofilin localized at the shaft region of comets (fig. S8A). In contrast, both N-WASP and cofilin localized to ruffles induced by PI(4,5)P<sub>2</sub> liberation (fig. S8B).

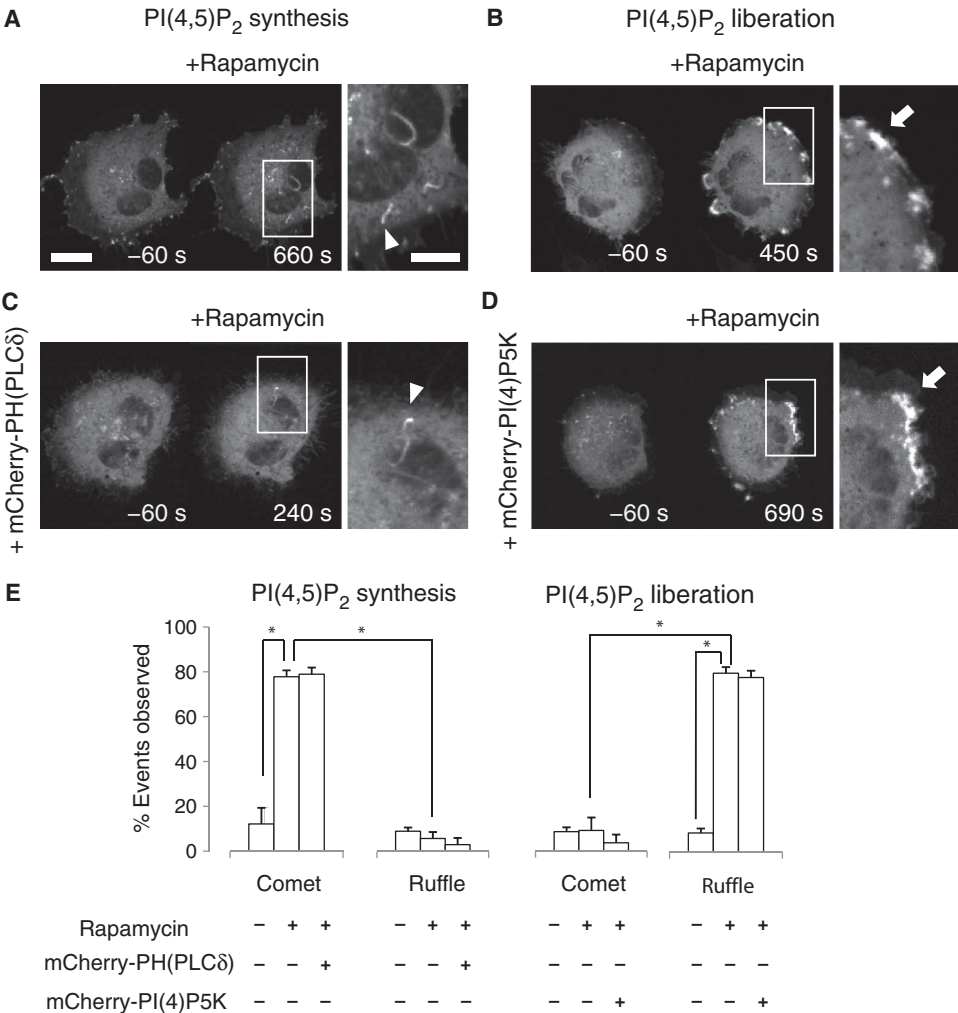


**Fig. 3. Distinct actin phenotypes induced by PI(4,5)P<sub>2</sub> synthesis and PI(4,5)P<sub>2</sub> liberation.** (A and C) Confocal fluorescence microscopy images of actin cytoskeleton before and after PI(4,5)P<sub>2</sub> synthesis in the absence (A) or presence (C) of overexpressed mCherry-PH(PLCδ). (B and D) Confocal fluorescence microscopy images of actin cytoskeleton before and after PI(4,5)P<sub>2</sub> liberation in the absence (B) or presence (D) of overexpressed mCherry-PI(4)P5K. Actin phenotypes were visualized by YFP-Evl. Images were collected at indicated time points. Right panel images highlight sites that show morphological changes [actin comets in (A) and (C), membrane ruffle in (B) and (D), highlighted by arrowheads and arrows, respectively]. Scale bars, 10 μm [representing (A) to (D)]. (E) Quantification of actin phenotypes (percent of cells showing comets and ruffles) induced by PI(4,5)P<sub>2</sub> manipulation. Values represent means ± SEM (n ≥ 30 cells from three independent experiments). \*P < 0.01. All P values are summarized in table S3.

**Endocytosis is required for PI(4,5)P<sub>2</sub>-induced actin remodeling** PI(4,5)P<sub>2</sub> also interacts with dynamin and promotes endocytosis (36), and actin comets are closely associated with regions of endocytic and exocytic activity (30). To investigate the possible role of membrane trafficking in the actin phenotypes we observed in response to PI(4,5)P<sub>2</sub> manipulation, we used a dominant-negative mutant form of dynamin 2 [Dyn2(K44A)] to inhibit endocytosis. Dyn2(K44A) significantly inhibited the formation of PI(4,5)P<sub>2</sub> synthesis-induced actin comets (Fig. 5A, P < 0.01; see table S3), but not that of PI(4,5)P<sub>2</sub> liberation-induced ruffles (Fig. 5B), suggesting that synthesis of PI(4,5)P<sub>2</sub> triggers endocytosis through dynamin. If PI(4,5)P<sub>2</sub> liberation induces endocytosis, this process is not required for the subsequent ruffling activity.

Collectively, our results suggested a working model for distinct roles for PI(4)P and PI(4,5)P<sub>2</sub> in actin remodeling by phosphoinositides (Fig. 5C). In this model, a PI(4,5)P<sub>2</sub> increase alone is sufficient to trigger membrane ruffling through activation

of the Rac and Cdc42 pathway. In contrast, PI(4,5)P<sub>2</sub> increase combined with a PI(4)P reduction drives actin comet formation in a manner that requires two signaling processes: PI(4,5)P<sub>2</sub>-induced endocytosis and PI(4)P-

mediated activation of the RhoA-ROCK pathway. Our model predicts that a decrease in PI(4)P alone will not elicit comets or ruffles. To test this, we treated cells with wortmannin, which decreases PI(4)P at the PM but not

PI(4,5)P<sub>2</sub> (20, 37), although wortmannin is also a potent inhibitor of phosphatidylinositol 3-kinase (PI3K). Consistent with the model, we did not observe comets or ruffles in response to wortmannin treatment (fig. S9).

Dynamin associates with the head region of actin comets (38, 39), raising the possibility that dynamin plays a role in comet formation through direct actin remodeling independent of its role in endocytosis. To further define the role of dynamin in comet formation, we rapidly induced endocytosis in the presence of active RhoA (fig. S10A) through a procedure that did not involve manipulation of phosphoinositides but relied on activation of the small GTPase Arf6 at the PM (fig. S10B). We recruited an Arf6 GEF (guanine nucleotide exchange factor, that is, an activator) fused to FKBP (FKBP-Sec7) to PM-targeted FRB, a manipulation that induced endocytosis (fig. S8, C and D). When we rapidly induced endocytosis with FKBP-Sec7 in the presence of constitutively active RhoA, we observed actin comet formation (Fig. 5D). We also observed actin comets in the presence of dominant-negative Rac1 (Fig. 5D), further supporting the reciprocal antagonism of RhoA and Rac GTPases (Fig. 5C).

## DISCUSSION

Mutually inhibitory Rac-RhoA signaling has been observed in biological processes including cell polarization, where such cross-talk helps to spatially segregate Rac and RhoA activity (40). Here, we found a signaling network dominated by strong mutual inhibition between components mediating actin comets (RhoA, ROCK, and endocytosis) and components mediating membrane ruffles (Rac and Cdc42). This crosstalk seems to function as a driving force to sharply define actin phenotypes on the basis of differential input signals originating from membrane lipids in a substrate-product relationship.

Under physiological conditions, there are four main ways whereby extracellular stimuli regulate PI(4,5)P<sub>2</sub> concentration. These are (i) PLC-mediated conversion of PI(4,5)P<sub>2</sub> into inositol phosphates and diacylglycerol, (ii) PI(4)P5K-mediated phosphorylation of PI(4)P, (iii) PI3K-mediated phosphorylation of PI(4,5)P<sub>2</sub>, and (iv) masking and unmasking of PI(4,5)P<sub>2</sub> by binding proteins such as myristoylated alanine-rich C-kinase substrate (5). Each mode is associated with

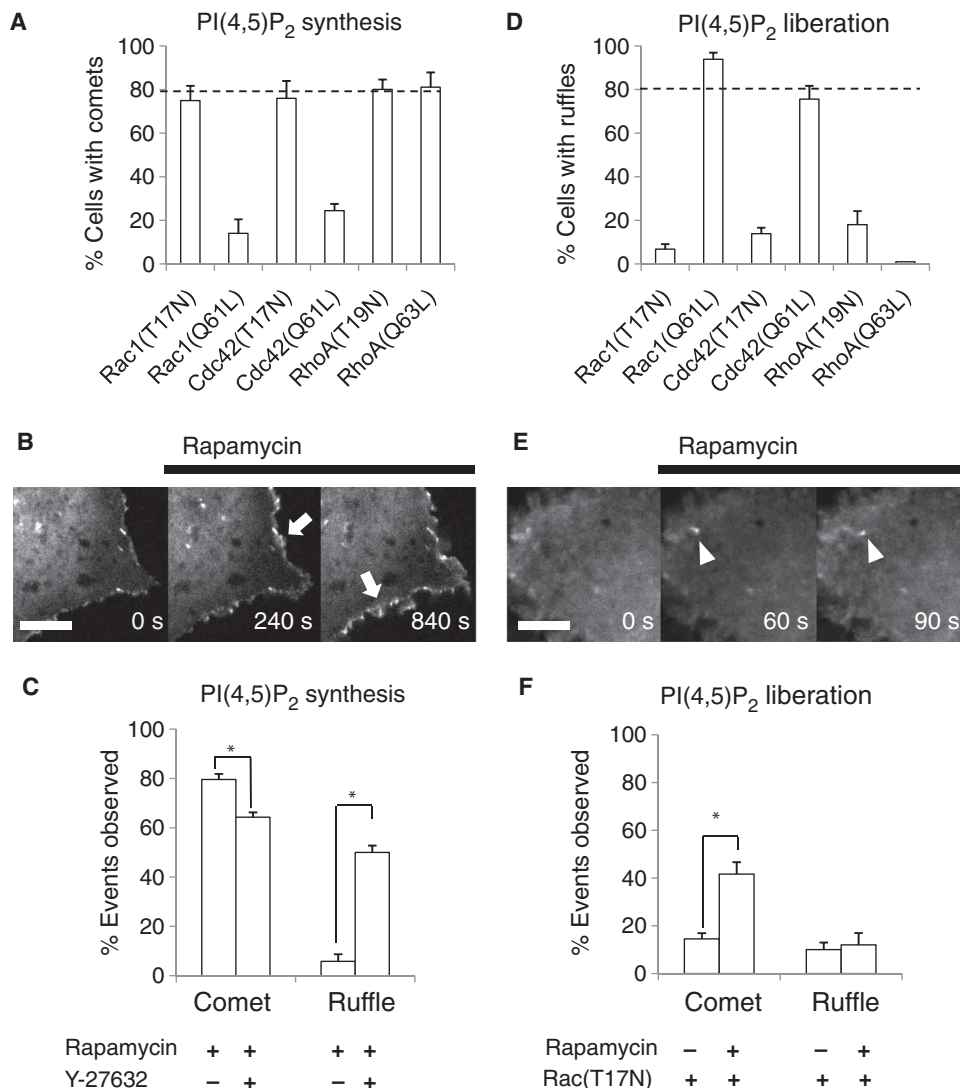


**Fig. 4.** Crosstalk between Rho GTPases regulates PI(4,5)P<sub>2</sub>-induced actin remodeling. (A and D) Effect of dominant mutants of Rho GTPases on comet formation in response to PI(4,5)P<sub>2</sub> synthesis (A) or ruffle formation in response to PI(4,5)P<sub>2</sub> liberation (D). The bar graphs represent scoring of actin phenotype in cells expressing CFP-FKBP-PI(4)P5K, Lyn<sub>11</sub>-FRB, YFP-Evl, and mCherry-tagged dominant-negative or constitutively active Rho GTPases (A) and CFP-FKBP-PH(PLCδ), mCherry-FRB-MoA and YFP-tagged dominant-negative or constitutively active Rho GTPase (D). The following dominant mutants were used: constitutively active: RacQ61L, Cdc42Q61L, RhoAQ63L; dominant negative: RacT17N, Cdc42T17N, RhoAT19N. Values represent means ± SEM (*n* ≥ 30 cells from three to four independent experiments). (B to F) Conversion of actin phenotypes induced by perturbation of Rho GTPase signaling. Confocal fluorescence microscopy images of actin cytoskeleton in COS-7 cells before and after PI(4,5)P<sub>2</sub> synthesis in the presence of Y-27632 (B) or PI(4,5)P<sub>2</sub> liberation in the presence of Rac(T17N) (E). Actin comets and membrane ruffle are highlighted by arrowheads and arrows, respectively. Scale bars, 10 μm. The observed actin phenotypes were quantified by counting the number of cells showing comets or ruffles under these conditions (C and F). Values represent means ± SEM (*n* ≥ 30 cells from three independent experiments). \**P* < 0.01. Single-letter abbreviations for the amino acid residues are as follows: L, Leu; N, Asn; Q, Gln; and T, Thr. All *P* values are summarized in table S3.

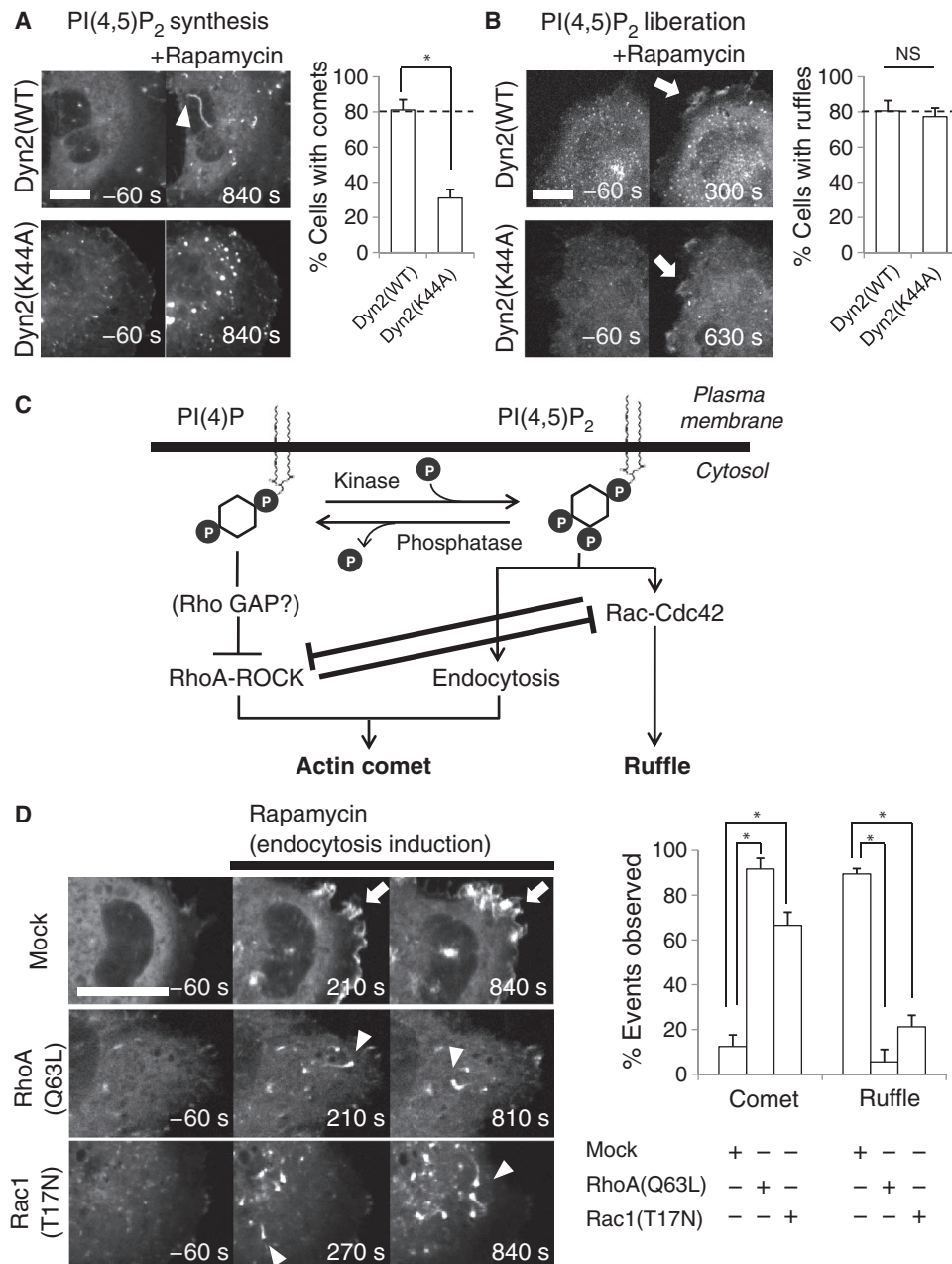


**Fig. 5.** Endocytosis regulates PI(4,5)P<sub>2</sub>-induced actin remodeling. (**A** and **B**) Confocal fluorescence microscopy images of COS-7 cells expressing either wild-type [Dyn2(WT), top panels] or dominant-negative [Dyn2(K44A), bottom panels] dynamin2 before and after PI(4,5)P<sub>2</sub> synthesis: PI(4,5)P<sub>2</sub> synthesis (**A**) and PI(4,5)P<sub>2</sub> liberation (**B**). Images are from YFP-Evl (**A**) or YFP-labeled Dyn2(WT) and Dyn2(K44A) (**B**). The observed actin phenotypes were quantified by counting the number of cells showing comets in response to PI(4,5)P<sub>2</sub> synthesis (**A**) or ruffles in response to PI(4,5)P<sub>2</sub> liberation (**B**). (**C**) Proposed model for the distinct actin phenotypes elicited by PI(4)P and PI(4,5)P<sub>2</sub>. (**D**) Reconstituting actin comet formation. Confocal fluorescence microscopy images of actin cytoskeleton of cells expressing inactive “Mock” protein (mCherry, top rows), RhoA(Q63L) (middle rows), or Rac1(T17N) (bottom rows) before and after rapid activation of Arf6. Actin comets and membrane ruffle are highlighted by arrowheads and arrows, respectively. Scale bars, 20  $\mu$ m. The observed actin phenotypes were quantified on the right by counting the number of cells showing comets or ruffles under these conditions. Values represent means  $\pm$  SEM ( $n \geq 30$  cells from three independent experiments). \* $P < 0.01$ . NS, not significant. Single-letter abbreviations for the amino acid residues are as follows: A, Ala, and K, Lys. All  $P$  values are summarized in table S3.

a unique combination of changes in the concentration of lipid products. Previous work has shown that decreased PI(4,5)P<sub>2</sub> concentration in response to acetylcholine receptor stimulation [mode (i)] deactivates ion channel activity (12). Here, we manipulated PI(4,5)P<sub>2</sub> synthetically to mimic modes (ii) and (iv) and found that PI(4)P and PI(4,5)P<sub>2</sub> play distinct roles in remodeling of the actin cytoskeleton. Our findings indicate that the consequence of an increase in PI(4,5)P<sub>2</sub> will depend on accompanying changes in different but closely related signaling molecules such as PI(4)P. Such a combinatorial regulation of downstream signals may at least partly explain the ability of a limited set of membrane lipids to exhibit such functional diversity.

Our model proposes that RhoA and ROCK signaling are activated downstream of PI(4)P. There seems to be no report of direct regulation of RhoA by PI(4)P. However, there are dozens of GEFs and GAPs for RhoA that contain lipid-binding domains (41), making them ideal candidates for PI(4)P-mediated RhoA regulation. Indeed, phospholipids have been reported to modulate the activity of p190 Rho GAP, one of the Rho GAPs (42). PI(4)P has long been viewed as a precursor of PI(4,5)P<sub>2</sub> and has only recently begun to be appreciated as a signaling molecule (17). Our data provide support for such a role.

Lowe syndrome is a genetic disease with defective 5-phosphatase activity for PI(4,5)P<sub>2</sub> that causes various developmental defects including eye, kidney, and brain problems. Of particular note, actin comets have been observed in fibroblasts from Lowe syndrome patients (43). These fibroblasts also exhibit cell migration defects (44). Because membrane ruffles offer the driving force for the cell motility, it is possible that the cell migration defects of these fibroblasts are due to a lack of ruffles through the mutual inhibition between actin comets and ruffles. Our study provides not only a powerful technology for probing the complexity of phosphoinositide signaling but also insights into the molecular mechanism of this currently incurable disease.

## MATERIALS AND METHODS

### Cell culture, transfection, and time-lapse fluorescence imaging

Culture of HeLa, tsA201, and NIH 3T3 cells was performed as described previously



(12, 45). HEK293 and COS-7 cells were maintained in DMEM (Dulbecco's modified Eagle's medium; Gibco) supplemented with 10% (v/v) fetal calf serum, penicillin (50 U/ml), and streptomycin (50 µg/ml). Cells were passaged every other day. Plasmid transfection of COS-7, HeLa, HEK293, and NIH 3T3 cells was performed with Lipofectamine 2000. After plating on poly-L-lysine-coated coverslips, all cells were maintained in DMEM supplemented with 10% fetal bovine serum for 12 to 24 hours before fluorescence imaging started. Typically, we took images every 15 s at room temperature and processed them with analysis software (Metamorph, Molecular Devices). In all experiments concerning PI(4,5)P<sub>2</sub>, cells were incubated for ≥3 hours in serum-free conditions before imaging. Phalloidin staining was conducted as follows: Cells were incubated with 100 nM rapamycin for 15 min at room temperature before fixation with 1% glutaraldehyde. The cells were then stained with Alexa 488-phalloidin with 0.1% Triton X-100.

### Confocal fluorescence microscopy

Time-lapse live-cell imaging by means of the confocal fluorescence microscope was conducted as previously described (16). Briefly, CFP and YFP excitations were conducted with helium-cadmium laser and argon laser (CVI-Melles Griot), respectively. The two lasers were fiber-coupled (OZ Optics) to the spinning disk confocal unit (CSU10; Yokogawa) mounted with dual dichroic mirrors for CFP and YFP (Semrock). The lasers were processed with appropriate filter sets for CFP and YFP (Chroma Technology) to capture fluorescence images with a charge-coupled device (CCD) camera (Orca ER, Hamamatsu Photonics) driven by Metamorph 7.5 imaging software (Molecular Devices). Images were taken with a 40× objective [Zeiss, numerical aperture (NA) = 1.30] mounted on an inverted Axiovert 200 microscope (Zeiss).

### TIRF microscopy

TIRF imaging was done with a Zeiss Axio Observer microscope (46). The excitation laser was a Coherent Sapphire (488 nm, 50 mW). The laser was coupled to a Zeiss TIRF slider via fiber optics (kineFLEX, Point Source). A Z488RDC dichroic mirror (Chroma Technology) was used to reflect the incoming laser onto a Zeiss A-Plan 100× objective (NA = 1.45). An ET525/50 emission filter was used for GFP-PH(OSBP) fluorescence detection (Chroma Technology). An EMCCD camera (ImagEM C9100-13; Hamamatsu Photonics) was used as detector. For detection of dim signals, the EMCCD gain was set to maximal. The camera was maintained at −85°C during the experiment by means of a JULABO HF25-ED heating and refrigerated circulator (JD Instruments). A Uniblitz LS6ZM2 shutter controlled by VCM-D1 (Vincent Associates) was integrated between the laser head and the fiber launcher to control the laser. Data were acquired with SlideBook (Intelligent Imaging Innovations).  $F/F_0$  traces were calculated from the TIRF signal intensity ( $F$ ) of GFP-PH(OSBP), averaged over the region of interest, and the initial fluorescence intensity ( $F_0$ ).

### Electrophysiology

KCNQ currents were recorded as previously (12, 22) in whole-cell, gigaseal voltage clamp of tsA201 cells transiently transfected with either KCNQ2 and KCNQ3 or KCNQ4 K channel subunits. The internal solution contained 175 mM KCl, 5 mM MgCl<sub>2</sub>, 5 mM Hepes, 0.1 mM K<sub>4</sub>BAPTA [1,2-bis(2-aminophenoxy)ethane-*N,N,N',N'*-tetraacetic acid, tetrapotassium salt], 3 mM Na<sub>2</sub>ATP, and 0.1 mM Na<sub>3</sub>GTP, pH 7.4 (KOH). The external solution contained 160 mM NaCl, 2.5 mM KCl, 2 mM CaCl<sub>2</sub>, 1 mM MgCl<sub>2</sub>, 10 mM Hepes, and 8 mM glucose, pH 7.4 (NaOH). Recordings used an EPC9 amplifier with Patchmaster 2.35 software (HEKA). Currents were filtered at 2.9 kHz. Sample intervals were 200 µs. Holding potential was −60 mV. KCNQ current was quantified by measuring tail

currents: Every 5 s, the membrane potential was depolarized to −20 mV for 300 ms and then repolarized to −60 mV. KCNQ currents activate slowly upon depolarization and deactivate slowly upon repolarization. Tail currents were measured by comparing current at 20 and 400 ms after repolarization to −60 mV. Simultaneously, we recorded FRET time courses as previously (22), using a two-channel photometry system with Polychrome IV (TILL Photonics) for excitation, a three-color dichroic mirror (89006bs CFP/YFP/mCherry, Chroma), and two photodiodes (TILL Photonics) with D480/40 and ET535/30 emission filters (Chroma). We recorded CFP<sub>C</sub> (440 nm excitation, 480 nm emission) and raw YFP<sub>C</sub> (440 nm excitation, 535 nm emission) every 5 s and calculated FRET<sub>r</sub> = YFP<sub>C</sub>/CFP<sub>C</sub> (in arbitrary units, AU) after subtracting background and correcting raw YFP<sub>C</sub> for CFP emission at 535 nm (YFP<sub>C</sub> = raw YFP<sub>C</sub> − 0.7CFP<sub>C</sub>).

### Modeling

A kinetic model of rapamycin-induced translocation and phosphoinositide metabolism was formulated as previously (22) as a compartmental model in the Virtual Cell framework (University of Connecticut). The Virtual Cell Model, Ueno2011, is publicly available at <http://www.vcell.org/> under shared models/bfalken. Model equations and initial conditions are listed in table S2.

### Design of constructs

Sequences encoding the human FRB (T2098L) domain of mTOR (mammalian target of rapamycin) and human FKBP12 were used for generating the following dimerization constructs. For CFP-FKBP-PH(PLCδ) and YFP-FKBP-PH(PLCδ) vector construction, YFP of YFP-PH(PLCδ) vector was replaced with a sequence encoding the Nhe I- and Eco RI-digested fragment of CFP-FKBP vector or YFP-FKBP vector. For Tubby-CFP-FKBP or Tubby-YFP-FKBP vector construction, a polymerase chain reaction (PCR) product encoding the Tubby domain of Tubby protein (a gift from A. Tinker, University College London, UK) (47) was digested with Eco RI and Bam HI and then inserted into the artificially introduced digestion site of the pEGFP-C1 vector in which enhanced green fluorescent protein (EGFP) was replaced with sequence encoding CFP-FKBP or YFP-FKBP. For CFP-FKBP-C2(Lact) and YFP-FKBP-C2(Lact) vector construction, the C2 domain of lactadherin from YFP-C2(Lact) (a gift from W. D. Heo, Korea Advanced Institute of Science and Technology, Korea) was subjected to PCR to provide Eco RI and Bam HI cleavage sites at its 5' and 3' ends. The PCR product was inserted using Eco RI and Bam HI restriction enzymes into CFP-FKBP and YFP-FKBP plasmids. For CFP-FKBP-C2(Lact) or YFP-FKBP-C2(Lact) vector construction, a PCR product encoding the C2 domain of lactadherin was digested with Eco RI and Bam HI and then inserted into the multiple cloning site of the pEGFP-C1 vector in which EGFP was replaced with sequence encoding CFP-FKBP or YFP-FKBP. For mCherry-PH(PLCδ) and mCherry-PI(4)P5K vector construction, YFP of YFP-PH(PLCδ) and CFP-FKBP of CFP-FKBP-PI(4)P5K (12) were replaced with sequence encoding mCherry. For the construction of CFP-FKBP-Sec7, the ArfGEF domain (Sec7: cytohesin-3 77-258aa) from human cytohesin-3 (a gift from T. Meyer, Stanford University, Palo Alto, CA; NM\_004227) was subcloned into Cerulean2-FKBP plasmid using Xho I and Kpn I after PCR was performed for Sec7 to have these restriction enzyme sites, and then inserted into the multiple cloning site of pEGFP C1 vector in which EGFP was replaced with sequence encoding Cerulean2-FKBP (Cerulean2 is a variant of CFP, a gift from M. A. Rizzo, University of Maryland, Baltimore, MD).

### Statistical analysis

Bars and markers in the figures represent means ± SEM. Statistical analysis was performed with an unpaired two-tailed Student's *t* test assuming



the two populations have the same variances. All analyses involved at least 30 cells in at least three separate experiments; statistical analyses and *P* values are summarized in table S3.

## SUPPLEMENTARY MATERIALS

www.sciencesignaling.org/cgi/content/full/4/203/ra87/DC1

Fig. S1. Kinetics of PH(PLC $\delta$ ) dynamics upon PDGF-induced PI(4,5)P<sub>2</sub> depletion.

Fig. S2. Quantitative analysis of PI(4,5)P<sub>2</sub> and model for phosphatidylinositol dynamics upon PI(4,5)P<sub>2</sub> manipulation.

Fig. S3. Actin phenotype upon recruitment of FKBP-tagged PI 5-kinase.

Fig. S4. Actin phenotype upon FKBP-tagged lipid binder sequestration.

Fig. S5. Confocal fluorescence microscopy images of cells after phalloidin staining upon PI(4,5)P<sub>2</sub> manipulation.

Fig. S6. Actin phenotypes in HeLa and HEK293 cells upon PI(4,5)P<sub>2</sub> synthesis and liberation.

Fig. S7. Evaluation of endogenous PI(4)P5K activity by means of KCNQ2/3 current in the presence of ROCK inhibitor.

Fig. S8. Actin phenotypes and actin-binding molecules.

Fig. S9. PI(4)P depletion does not induce actin phenotype.

Fig. S10. Synthetic reconstitution of actin comets.

Table S1. Initial conditions used for the model.

Table S2. Differential equations used for the model.

Table S3. Summary of statistical analyses, including *P* values.

Movie S1. Inducible recruitment of PI(4)P5K to plasma membrane.

Movie S2. Inducible sequestration of PH(PLC $\delta$ ) from plasma membrane.

Movie S3. PI(4,5)P<sub>2</sub> synthesis induces actin comets.

Movie S4. PI(4,5)P<sub>2</sub> liberation induces membrane ruffles.

## REFERENCES AND NOTES

- G. Di Paolo, P. De Camilli, Phosphoinositides in cell regulation and membrane dynamics. *Nature* **443**, 651–657 (2006).
- S. J. Field, N. Madson, M. L. Kerr, K. A. Galbraith, C. E. Kennedy, M. Tahiliani, A. Wilkins, L. C. Cantley, PtdIns(4,5)P<sub>2</sub> functions at the cleavage furrow during cytokinesis. *Curr. Biol.* **15**, 1407–1412 (2005).
- K. Ling, N. J. Schill, M. P. Wagoner, Y. Sun, R. A. Anderson, Movin' on up: The role of PtdIns(4,5)P<sub>2</sub> in cell migration. *Trends Cell Biol.* **16**, 276–284 (2006).
- T. F. Martin, PI(4,5)P<sub>2</sub> regulation of surface membrane traffic. *Curr. Opin. Cell Biol.* **13**, 493–499 (2001).
- S. McLaughlin, J. Wang, A. Gambhir, D. Murray, PIP<sub>2</sub> and proteins: Interactions, organization, and information flow. *Annu. Rev. Biophys. Biomol. Struct.* **31**, 151–175 (2002).
- B. C. Suh, B. Hille, Regulation of ion channels by phosphatidylinositol 4,5-bisphosphate. *Curr. Opin. Neurobiol.* **15**, 370–378 (2005).
- T. Yeung, B. Ozdamar, P. Paroutis, S. Grinstein, Lipid metabolism and dynamics during phagocytosis. *Curr. Opin. Cell Biol.* **18**, 429–437 (2006).
- H. L. Yin, P. A. Janmey, Phosphoinositide regulation of the actin cytoskeleton. *Annu. Rev. Physiol.* **65**, 761–789 (2003).
- M. Santarius, C. H. Lee, R. A. Anderson, Supervised membrane swimming: Small G-protein lifeguards regulate PIPK signalling and monitor intracellular PtdIns(4,5)P<sub>2</sub> pools. *Biochem. J.* **398**, 1–13 (2006).
- H. J. McCrea, P. De Camilli, Mutations in phosphoinositide metabolizing enzymes and human disease. *Physiology* **24**, 8–16 (2009).
- L. M. Ooms, K. A. Horan, P. Rahman, G. Seaton, R. Gurung, D. S. Kethesparan, C. A. Mitchell, The role of the inositol polyphosphate 5-phosphatases in cellular function and human disease. *Biochem. J.* **419**, 29–49 (2009).
- B.-C. Suh, T. Inoue, T. Meyer, B. Hille, Rapid chemically induced changes of PtdIns(4,5)P<sub>2</sub> gate KCNQ ion channels. *Science* **314**, 1454–1457 (2006).
- P. Várnai, B. Thyagarajan, T. Rohacs, T. Balla, Rapidly inducible changes in phosphatidylinositol 4,5-bisphosphate levels influence multiple regulatory functions of the lipid in intact living cells. *J. Cell Biol.* **175**, 377–382 (2006).
- S. Etienne-Manneville, A. Hall, Rho GTPases in cell biology. *Nature* **420**, 629–635 (2002).
- C. J. Merrifield, S. E. Moss, C. Ballestrem, B. A. Imhof, G. Giese, I. Wunderlich, W. Almers, Endocytic vesicles move at the tips of actin tails in cultured mast cells. *Nat. Cell Biol.* **1**, 72–74 (1999).
- T. Komatsu, I. Kukelyansky, J. M. McCaffery, T. Ueno, L. C. Varela, T. Inoue, Organelle-specific, rapid induction of molecular activities and membrane tethering. *Nat. Methods* **7**, 206–208 (2010).
- G. D'Angelo, M. Vicinanza, A. Di Campli, M. A. De Matteis, The multiple roles of PtdIns(4)P—Not just the precursor of PtdIns(4,5)P<sub>2</sub>. *J. Cell Sci.* **121**, 1955–1963 (2008).
- U. Golebiewska, M. Nyako, W. Woturski, I. Zaitseva, S. McLaughlin, Diffusion coefficient of fluorescent phosphatidylinositol 4,5-bisphosphate in the plasma membrane of cells. *Mol. Biol. Cell* **19**, 1663–1669 (2008).
- G. van Meer, D. R. Voelker, G. W. Feigenson, Membrane lipids: Where they are and how they behave. *Nat. Rev. Mol. Cell Biol.* **9**, 112–124 (2008).
- G. R. Hammond, G. Schiavo, R. F. Irvine, Immunocytochemical techniques reveal multiple, distinct cellular pools of PtdIns4P and PtdIns(4,5)P<sub>2</sub>. *Biochem. J.* **422**, 23–35 (2009).
- B. H. Falkenburger, J. B. Jensen, B. Hille, Kinetics of M<sub>1</sub> muscarinic receptor and G protein signaling to phospholipase C in living cells. *J. Gen. Physiol.* **135**, 81–97 (2010).
- B. H. Falkenburger, J. B. Jensen, B. Hille, Kinetics of PIP<sub>2</sub> metabolism and KCNQ2/3 channel regulation studied with a voltage-sensitive phosphatase in living cells. *J. Gen. Physiol.* **135**, 99–114 (2010).
- C. C. Hernandez, B. Falkenburger, M. S. Shapiro, Affinity for phosphatidylinositol 4,5-bisphosphate determines muscarinic agonist sensitivity of Kv7 K<sup>+</sup> channels. *J. Gen. Physiol.* **134**, 437–448 (2009).
- B.-C. Suh, B. Hille, Recovery from muscarinic modulation of M current channels requires phosphatidylinositol 4,5-bisphosphate synthesis. *Neuron* **35**, 507–520 (2002).
- H. Zhang, L. C. Craciun, T. Mirshahi, T. Rohacs, C. M. Lopes, T. Jin, D. E. Logothetis, PIP<sub>2</sub> activates KCNQ channels, and its hydrolysis underlies receptor-mediated inhibition of M currents. *Neuron* **37**, 963–975 (2003).
- Y. Li, N. Gamper, D. W. Hilgemann, M. S. Shapiro, Regulation of Kv7 (KCNQ) K<sup>+</sup> channel open probability by phosphatidylinositol 4,5-bisphosphate. *J. Neurosci.* **25**, 9825–9835 (2005).
- A. Balla, G. Tuymetova, A. Tsiomenko, P. Várnai, T. Balla, A plasma membrane pool of phosphatidylinositol 4-phosphate is generated by phosphatidylinositol 4-kinase type-III  $\alpha$ : Studies with the PH domains of the oxysterol binding protein and FAPP1. *Mol. Biol. Cell* **16**, 1282–1295 (2005).
- M. Krause, E. W. Dent, J. E. Bear, J. J. Loureiro, F. B. Gertler, Ena/VASP proteins: Regulators of the actin cytoskeleton and cell migration. *Annu. Rev. Cell Dev. Biol.* **19**, 541–564 (2003).
- S. Santagata, T. J. Boggon, C. L. Baird, C. A. Gomez, J. Zhao, W. S. Shan, D. G. Myszka, L. Shapiro, G-protein signaling through tubby proteins. *Science* **292**, 2041–2050 (2001).
- A. L. Rozelle, L. M. Machesky, M. Yamamoto, M. H. Driessens, R. H. Insall, M. G. Roth, K. Luby-Phelps, G. Marriott, A. Hall, H. L. Yin, Phosphatidylinositol 4,5-bisphosphate induces actin-based movement of raft-enriched vesicles through WASP-Arp2/3. *Curr. Biol.* **10**, 311–320 (2000).
- D. A. Zacharias, J. D. Violin, A. C. Newton, R. Y. Tsien, Partitioning of lipid-modified monomeric GFPs into membrane microdomains of live cells. *Science* **296**, 913–916 (2002).
- J. B. Jensen, J. S. Lyssand, C. Hague, B. Hille, Fluorescence changes reveal kinetic steps of muscarinic receptor-mediated modulation of phosphoinositides and Kv7.2/7.3 K<sup>+</sup> channels. *J. Gen. Physiol.* **133**, 347–359 (2009).
- Y. Takai, T. Sasaki, T. Matozaki, Small GTP-binding proteins. *Physiol. Rev.* **81**, 153–208 (2001).
- M. Yamamoto, D. H. Hilgemann, S. Feng, H. Bito, H. Ishihara, Y. Shibasaki, H. L. Yin, Phosphatidylinositol 4,5-bisphosphate induces actin stress-fiber formation and inhibits membrane ruffling in CV1 cells. *J. Cell Biol.* **152**, 867–876 (2001).
- M. Symons, J. Settleman, Rho family GTPases: More than simple switches. *Trends Cell Biol.* **10**, 415–419 (2000).
- S. L. Schmid, M. A. McNiven, P. De Camilli, Dynamin and its partners: A progress report. *Curr. Opin. Cell Biol.* **10**, 504–512 (1998).
- S. Nakanishi, K. J. Catt, T. Balla, A wortmannin-sensitive phosphatidylinositol 4-kinase that regulates hormone-sensitive pools of inositolphospholipids. *Proc. Natl. Acad. Sci. U.S.A.* **92**, 5317–5321 (1995).
- E. Lee, P. De Camilli, Dynamin at actin tails. *Proc. Natl. Acad. Sci. U.S.A.* **99**, 161–166 (2002).
- J. D. Orth, E. W. Krueger, H. Cao, M. A. McNiven, The large GTPase dynamin regulates actin comet formation and movement in living cells. *Proc. Natl. Acad. Sci. U.S.A.* **99**, 167–172 (2002).
- S. Iden, J. G. Collard, Crosstalk between small GTPases and polarity proteins in cell polarization. *Nat. Rev. Mol. Cell Biol.* **9**, 846–859 (2008).
- S. Y. Moon, Y. Zheng, Rho GTPase-activating proteins in cell regulation. *Trends Cell Biol.* **13**, 13–22 (2003).
- E. Ligeti, M. C. Dagher, S. E. Hernandez, A. J. Koleske, J. Settleman, Phospholipids can switch the GTPase substrate preference of a GTPase-activating protein. *J. Biol. Chem.* **279**, 5055–5058 (2004).
- P. G. Allen, Actin filament uncapping localizes to ruffling lamellae and rocketing vesicles. *Nat. Cell Biol.* **5**, 972–979 (2003).
- B. G. Coon, D. Mukherjee, C. B. Hanna, D. J. Riese II, M. Lowe, R. C. Aguilar, Lowe syndrome patient fibroblasts display Ocr1-specific cell migration defects that cannot be rescued by the homologous Inpp5b phosphatase. *Hum. Mol. Genet.* **18**, 4478–4491 (2009).

45. T. Inoue, W. D. Heo, J. S. Grimley, T. J. Wandless, T. Meyer, An inducible translocation strategy to rapidly activate and inhibit small GTPase signaling pathways. *Nat. Methods* **2**, 415–418 (2005).
46. Y. Araki, D. T. Lin, R. L. Huganir, Plasma membrane insertion of the AMPA receptor GluA2 subunit is regulated by NSF binding and Q/R editing of the ion pore. *Proc. Natl. Acad. Sci. U.S.A.* **107**, 11080–11085 (2010).
47. K. V. Quinn, P. Behe, A. Tinker, Monitoring changes in membrane phosphatidylinositol 4,5-bisphosphate in living cells using a domain from the transcription factor tubby. *J. Physiol.* **586**, 2855–2871 (2008).

**Acknowledgments:** We thank T. Balla for the PH(OSBP) plasmid, T. Andrew for the Tubby plasmid, W. D. Heo for the dominant mutants of Rho GTPases and C2(Lact) plasmids, J. Donaldson for the dynamin2 (wild-type and K44A) plasmids, M. Rizzo for the mCerulean2 plasmid, and ARIAD Pharmaceuticals Inc. for FKBP and FRB plasmids. We extend our appreciation to R. Huganir and Y. Araki for help with TIRF measurements and also to D. Montell, A. Ewald, B. Hille, M. Fivaz, and Inoue lab members for valuable discussion and comments on the manuscript. **Funding:** Our research is supported by NIH grants

DK090868, MH084691, and GM092930 (to T.I.). T.U. is a recipient of a fellowship from the Japan Society for the Promotion of Science. B.H.F. is a long-term fellow of the Human Frontier Science Program and funded by NIH grant NS08174 (to B. Hille). The Virtual Cell is supported by NIH grant P41RR013186 from the National Center for Research Resources. **Author contributions:** T.U. and T.I. conceived the original idea of PI(4,5)P<sub>2</sub> manipulation techniques. T.U., B.H.F., C.P., and T.I. designed and conducted the experiments and analyzed the data. T.U., B.H.F., and T.I. wrote the manuscript. **Competing interests:** The authors declare that they have no competing interests.

Submitted 22 March 2011

Accepted 22 November 2011

Final Publication 13 December 2011

10.1126/scisignal.2002033

**Citation:** T. Ueno, B. H. Falkenburger, C. Pohlmeier, T. Inoue, Triggering actin comets versus membrane ruffles: Distinctive effects of phosphoinositides on actin reorganization. *Sci. Signal.* **4**, ra87 (2011).